




Design of a high-speed circular polarization converter with a large field of view and wavelength range

YANG YU,^{1,2}  ZHIBO SUN,³ QUANQUAN MU,^{1,2,*} HOI-SING KWOK,³ QIDONG WANG,^{1,2,4} CHENGLIANG YANG,^{1,2} SHIXIAO LI,^{1,2} WAN CHEN,^{1,2} AND TONGTONG HAN^{1,2}

¹State Key Laboratory of Applied Optics, Changchun Institute of Optics, Fine Mechanics and Physics, Chinese Academy of Sciences, 14 Changchun 130033, China

²University of Chinese Academy of Sciences, Beijing 100049, China

³State Key Laboratory of Advanced Displays and Optoelectronics Technologies, Hong Kong University of Science and Technology, Clear Water Bay, Kowloon, Hong Kong 999077, China

⁴qdwang@ciomp.ac.cn

*muquanquan@ciomp.ac.cn

Abstract: A high-speed circular polarization converter (CPC) with a wide field of view (FOV) and wavelength range is designed and fabricated in this paper. The multi-waveplate combined structure is applied to constitute the basic configuration of the CPC for broadening the wavelength range. An electrically suppressed helix ferroelectric liquid crystal (ESHFLC) material with fast response is used as a medium for dynamic polarization operation. The compensation films are used to expand the FOV by attaching to the configuration. The simulation results demonstrate that the optimized CPC structure can achieve over 97% orthogonal circular polarization conversion efficiency in 300 nm bandwidth at a 90° viewing cone for both working states. Finally, we have experiments and the results show well consistency with the theoretical results.

© 2023 Optica Publishing Group under the terms of the [Optica Open Access Publishing Agreement](#)

1. Introduction

As a new approach to the optical phase and polarization modulation, geometric phase devices (GPDs) [1] exhibit excellent performance. Benefiting from its excellent optical alignment property, the planar diffractive LC-based GPD [2–4] has great advantages of high efficiency, dynamic reconfigurable, and easy fabrication, which is one of the most important types of GPDs. The cascading combination of high-speed polarization converters and passive GPDs shows promising application performance in non-mechanical beam steering [5,6], polarization-based stereoscopic 3D displays and AR/VR displays [7–9]. Most optical systems usually require a broad wavelength range and a large FOV for many situations. The passive liquid crystal polarization elements can extend the viewing angle or bandwidth by forming a special structural distribution (twisted or chirped structure). A chirped polarized volume grating structure reported displays a diffraction efficiency of more than 80% by introducing a gradient pitch along the beam propagation direction with an angular bandwidth expanded from 18° to 54° [10]. The multi-layer twisted structure has been successfully applied in various LC-based GPDs to meet the application requirements of wave band and FOV [11–14]. In addition, the polarization-time multiplexing configuration can also be used to extend the FOV [15]. Overall, numerous efforts have been focused on the research of passive polarization elements, but the active liquid crystal polarization device is also an indispensable part of optical systems. Therefore, the design of dynamic CPCs is also a facing challenge to solving the restrictions of wave band and FOV for existing polarization elements.

Currently, the twisted nematic (TN) and parallel aligned (PA) LC devices have been reported polarization conversion. Zhuang et al. [16] proposed an achromatic polarization rotator consisting

of two PA cells and one TN cell, which could expand the wavelength range to 250 nm in the visible spectrum, but it is too complex to fabricate. Wu et al. [17] used two uniaxial compensation films to replace the PA cells, which can further broaden the wavelength range and simplify its manufacture, but both of them are not switchable. Subsequently, Wang et al. [18] optimized a broadband polarization switch consisting of an active TN cell and two passive uniaxial compensation films and achieved a limited FOV of $\pm 15^\circ$. Most of the polarization converters containing the TN cell are for linear polarization modulation, and the modulation of circular polarization state requires the addition of achromatic quarter-wave plates. Xiong et al. [19] introduced a CPC based on a TN cell and achromatic quarter-wave plates, which has an orthogonal conversion efficiency of 90% in the 465-630 nm wavelength range and $\pm 30^\circ$ FOV. However, due to the residual phase retardation caused by the LC layer near the substrates, the FOV performance was quite different for the two polarization states. FLC cell [20,21] can be regarded as an active waveplate with a reconfigurable optical axis, which can realize the consistent phase modulation for two polarization states. In addition, FLC materials have a much faster response capability than twisted nematic liquid crystal polymer materials, which is very essential for beam control in many scenarios. As a new type of FLC material, ESHFLC has great alignment quality and a low unwinding threshold voltage, which has proven its possibility for GPD applications [22].

In this paper, the designed CPC can achieve over 97% circular polarization conversion efficiency within 300 nm bandwidth at a view cone of 90° . We first briefly introduced its working principle part, including the basic CPC structure, the dynamic orthogonal polarization conversion process, and the compensation structure for wave band and FOV. Then we optimize the structure and carry out experiments. The experimental results show good agreement with the simulation. Finally, we explain the degradation of conversion efficiency under a large incident angle.

2. Design

The CPC device is used for circularly polarized light conversion and can operate between switching state and holding state respectively. The basic structure of the device can be simplified as a reformed QHQ configuration, which includes two quarter-wave plates (Q layer) and one half-wave plate (H layer) as shown in Fig. 1(a). Each Q layer can be considered as a combination of “+C film” and “+A film” for FOV and wavelength range compensation. The optical axes of “+A film” and “+C film” are parallel and perpendicular to the substrate respectively. “+C film” is selected to compensate for the FOV of the broadband structure mainly because it has consistent retardation under different incident azimuth angles. Besides, the achromatic performance of the reformed QHQ configuration at normal incidence is not influenced by the introduced “+C film” because of the zero retardation. The H layer is an ESHFLC cell located in the middle of the device and acts as a uniaxial phase retarder with a switchable optical axis. The alignment of the ESHFLC helix axis is along the x-axis. In this configuration, the CPC device can be equivalent to an achromatic half-wave plate in the switching state and an achromatic full-wave plate in the holding state according to the Jones matrix calculation [21], the optical axis distributions are shown in Fig. 1(b).

The Poincaré sphere is used to visualize the polarization evolution process under different wavelengths and FOVs. The red dash path S_i -A-B- S_o in Fig. 2(a) shows the polarization transition trace from the right-handed circularly polarization state S_i (North Pole) to the left-handed circularly polarization state S_o (South Pole), corresponding to the switching state. The path S_i -A-B'- S_o' shows the polarization transition trace from the right-handed circular polarization state S_i (North Pole) to the right-handed circular polarization S_o' (North Pole), corresponding to the holding state. The rainbow arcs A, B, B', S_o , and S_o' indicate the dispersion generated during the polarization evolution. The length of S_o and S_o' represents the final dispersion performance. As is shown in Fig. 2(b), the polarization evolution process denotes the output polarization in different azimuths at a certain wavelength and incident angle. The closed curves L-1Q, L-2H,

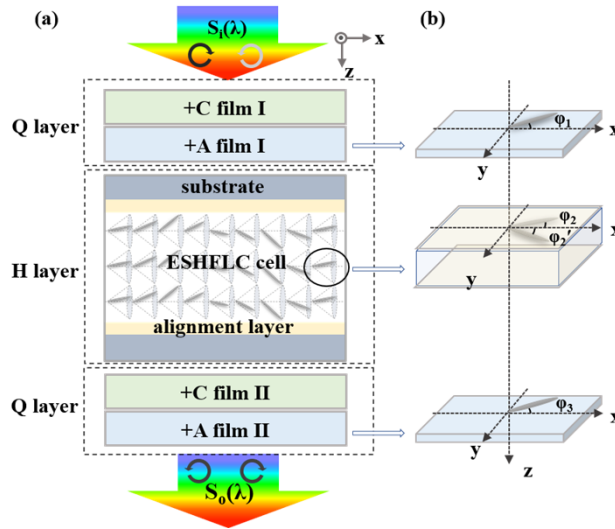


Fig. 1. (a) Illustration of the CPC design. (b) Optical axis distribution. $\phi_1 = \phi_3$, represents the optical axis angle of uniaxial film; ϕ_2 and ϕ_2' represent the optical axis angles of two working states.

and L-3Q indicate the polarization states for all azimuth angles during the switching process. The size of the closed curve L-3Q represents the final FOV performance.

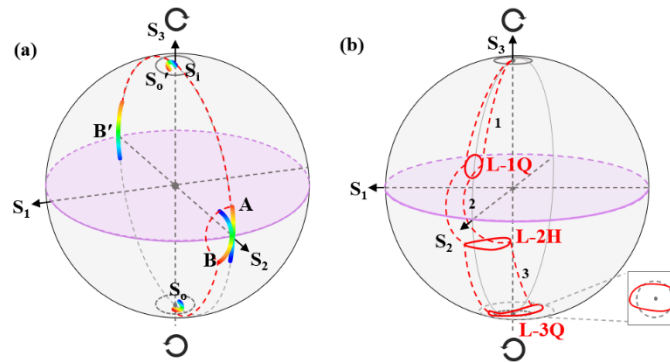


Fig. 2. Polarization evolution process on the Poincaré sphere. (a) Polarization state transition of different wavelengths. (b) Polarization state transition of different FOVs.

3. Simulation and experiment

Simulations and experiments are carried out to verify the proposed CPC configuration. The finite element method (FEM) is used to analyze the proposed CPC device and the nonlinear constraint-optimization algorithm is used to optimize its structure parameters. The conversion efficiency η is defined according to Stokes parameter S_3 for evaluation:

$$\eta = \frac{1 \mp S_3}{2}. \tag{1}$$

“-” represents the switching state, and “+” represents the holding state. Stokes parameter S_3 is the circular polarization component of polarized light. Then the merit function can be expressed by:

$$F = \frac{\sum_{k=1}^K \left(\sum_{i=1}^N \left(\sum_{j=1}^M \left| 1 - \frac{S_3(\lambda_k, \theta_i, \psi_j)}{2} \right|^2 \right) \right)}{N \times M - 1}. \quad (2)$$

F is a wavelength-dependent and FOV-dependent function, λ_k , θ_i and ψ_j represent the discrete wavelength, incident angle, and azimuth angle used for evaluation respectively. 460 nm, 530 nm, and 630 nm wavelengths are selected as the optimized central wavelengths during the visible spectrum. The dispersion of the 5-layer structure in the simulation is considered as $\Delta n = 0.08423 + 5961/\lambda^2$. The angular optimization of the incident angle is considered from 0° to 45° and the azimuth angle is from 0° to 360° . By the discrete numerical calculation of the merit function in the angular interval above, we optimize the cumulative loss function until $\sim 10^{-6}$. The FOV performance of two working states calculated within $\pm 45^\circ$ incident angle for three wavelengths is portrayed in Fig. 3. The simulation results manifest that the design can achieve over 97% conversion efficiency, and both operating states present almost the same optical performance of the wave band and the FOV.

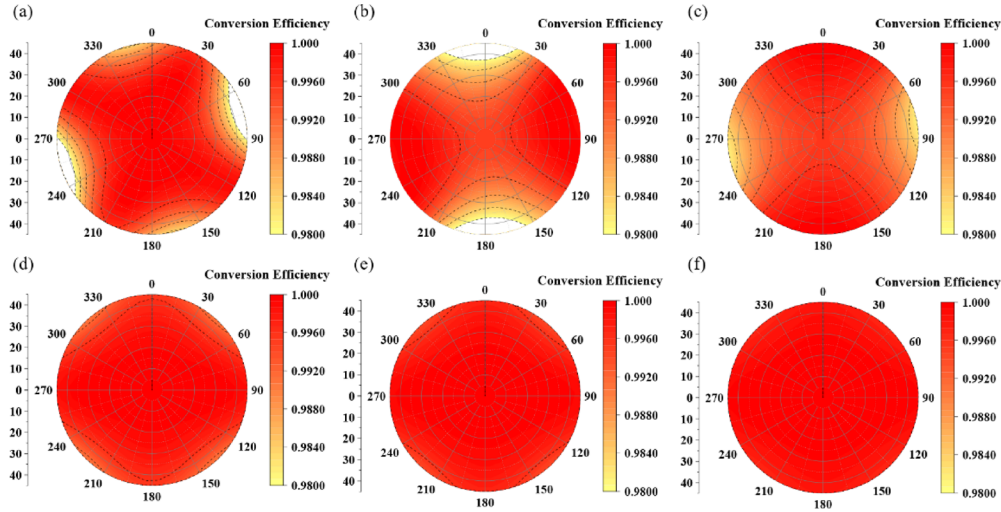


Fig. 3. Compensation results of the large FOV and broadband CPC. Switching state: (a) 460 nm. (b) 530 nm. (c) 630 nm. Holding state: (d) 460 nm. (e) 530 nm. (f) 630 nm.

Then we fabricated a CPC device to experimentally verify the reliability of the optimization. During the process of fabrication, the compensation films and the ferroelectric liquid crystal layer are assembled with equivalent simulated retardation values above. The materials involved in the experiment of “+A film” and “+C film” are polycarbonate and liquid crystal polymer respectively. FD4004N (from Dai-Nippon Ink and Chemicals) was used as the switchable layer material. Two optically flat indium tin oxide-coated glass plates having enough conducting area were used as electrodes for preparing a sandwich-type sample holder with a cell gap needed. Nylon 6 was deposited on the substrate by spin-coating with 3000 rpm for 2 mins. Soft baking at 100°C for 10 mins and hard baking at 180°C for 1 hour were followed then. Later, both the substrates were rubbed unidirectionally and assembled to make the FLC cell. After that, we attached the compensation films to both sides of the prepared ESHFLC cell according to the optical axis angle of the simulation parameters, and the Refractive Index (Matching) Liquids were used to fill into the interlayer gap between surfaces to reduce interlayer reflection. Table 1 shows the optimized

thickness parameters and the experimental retardation parameters at 550 nm of the CPC design. The optical layout of circular polarization conversion efficiency measurement with a profile display of the CPC device is shown in Fig. 4. In the measuring optical path, the achromatic quarter-wave plate (AQWP05M-580) was used to generate the incident circular polarized light. The combination of the achromatic quarter-wave plate (AQWP05M-580), polarizer (P), and optical power meter (OPM) was used to detect the polarization state after the light passes through the CPC device. For the entire FOV performance measurement, a two-dimensional rotator has been used to change the incident angle from 0° to 45° and the azimuth angle from 0° to 360° . The experiment results demonstrated in Fig. 5 exhibit well agreement with simulations when the incident angle is no more than 30° . The circularly polarized conversion efficiency degradation at larger incident angles than 30° is discussed subsequently. In addition, we measured the switching time as shown in Fig. 6. The dynamic CPC can achieve an average switching time of approximately $150\mu\text{s}$ driven by an AC voltage of 10 V amplitude at 500 Hz.

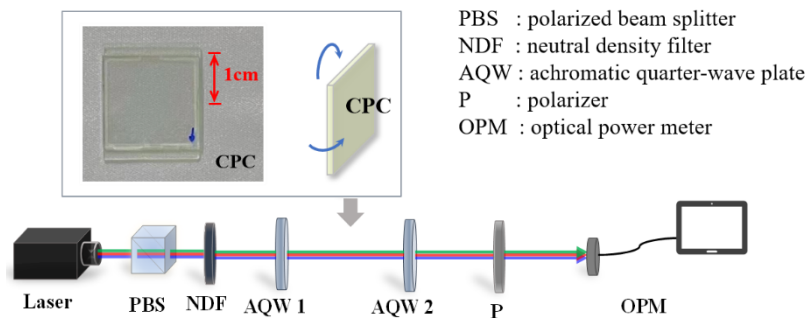


Fig. 4. Circular polarization conversion efficiency measurement setup.

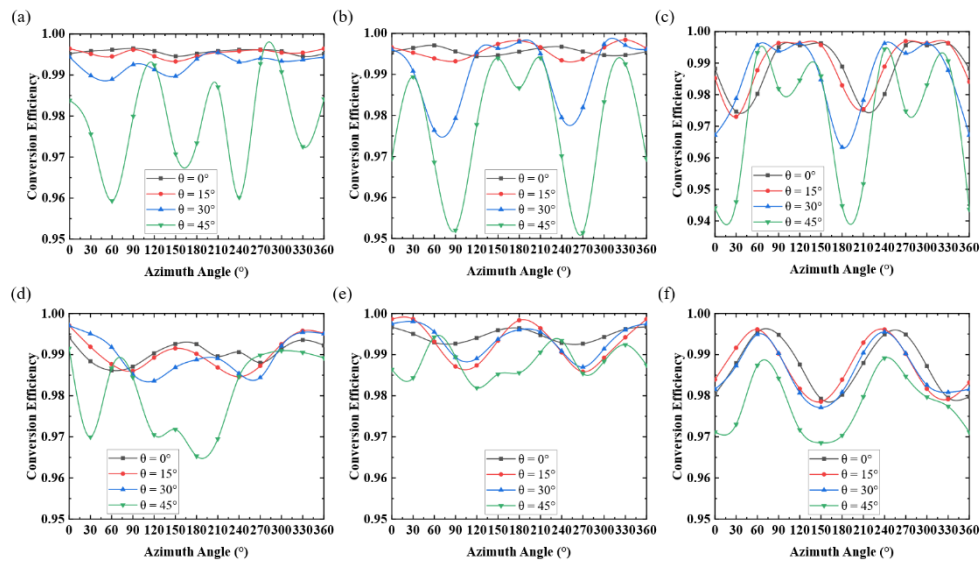


Fig. 5. Conversion efficiency of the CPC. Switching state: (a) 450 nm. (b) 532 nm. (c) 633 nm. Holding state: (d) 450 nm. (e) 532 nm. (f) 633 nm.

As for the incident angle of 45° , the conversion efficiency degradation is mainly caused by the alignment deviations among different layers, especially for the dynamic switching layer.

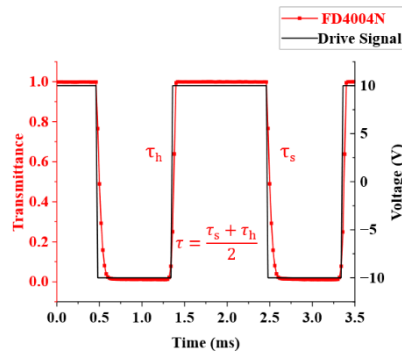


Fig. 6. Switching time between two working states. τ_h is the response time from the switching state to the holding state, and τ_s is the response time from the holding state to the switching state

Table 1. Large FOV and broadband CPC Design

Layers	L-1C	L-2A	L-3FLC	L-4C	L-5A
Thickness $d(\mu\text{m})$	1.08	1.23	2.43	1.17	1.22
Azimuth Angle $\varphi(^{\circ})$	-	0	-43/-90	-	0
Retardation $\Gamma(\text{nm})$	112	128	253	122	127

Theoretical simulation at 460 nm illustrates that the optical axis deviation of the ferroelectric liquid crystal layer (H layer) has the greatest influence, as demonstrated in Fig. 7(a-b), and the same is true at other wavelengths. The relationship between the conversion efficiency (PV value of curves in Fig. 7(a-b) and the optical axis deviation is shown in Fig. 7(c-d), which indicates that the angular deviations have a greater influence on the switching state. The angular deviations

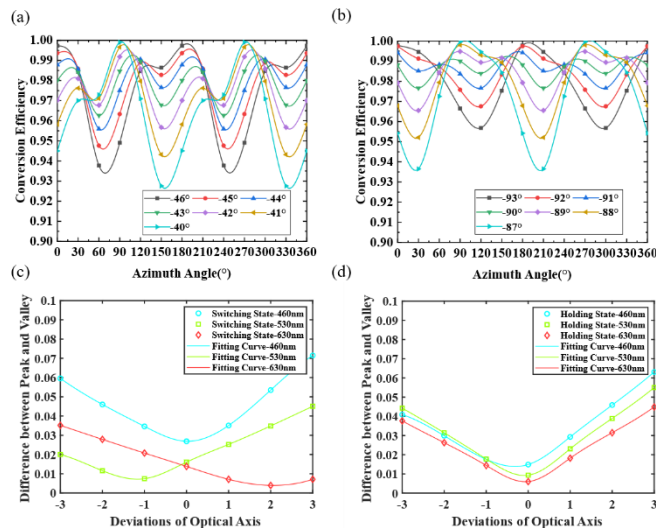


Fig. 7. Optical axis angle deviations of the switchable layer. (a) conversion efficiency calculation of the switching state at 460 nm. (b) conversion efficiency calculation of the holding state at 460 nm. (c) PV values of the switching state. (d) PV values of the holding state.

should be controlled within the deviation range of $\pm 1^\circ$ in case of the conversion efficiency degradation is less than 4% for the switching state and 3% for the holding state respectively. Besides, the simulation shows that conversion efficiency at a long wavelength will decrease if retardation bias are existing, as shown in Fig. 8, the impacts on the two operating states are significantly different, it is obvious to see that the switching state is more sensitive to the bias than the holding state.

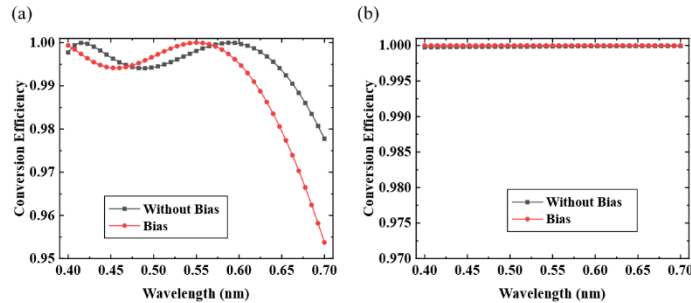


Fig. 8. Retardation bias of the CPC. (a) Switching state. (b) Holding state.

4. Conclusion

We experimentally and theoretically demonstrated a high-speed broadband wide-view CPC design in this paper, which is mainly achieved by mutual phase compensation among all the retardation films. It can operate with a sub-millisecond response time and keep over 97% conversion efficiency within a 300 nm wavelength range at a 90° view cone and the experiments show consistency with the theoretical simulations. Furthermore, it has almost the same optical performance for two working states. The CPC structure can also be applied in different application fields by changing optimized parameters. The properties of achromatism, wide-FOV, and high-speed switching exhibit excellent cooperation of GPDs and CPCs, and make the combination greatly promising in beam modulation for the futural optical system.

Funding. National Key Research and Development Program of China (2021YFB3600300); National Natural Science Foundation of China (11974345, 61975202, U2241224).

Acknowledgments. This research is supported by the Changchun Institute of Optics, Fine Mechanics and Physics, Chinese Academy of Sciences, and the State Key Laboratory of Advanced Displays and Optoelectronics Technologies (HKUST).

Disclosures. The authors declare no conflicts of interest.

Data Availability. No data were generated or analyzed in the presented research.

References

1. J. Anandan, "The geometric phase," *Nature* **360**(6402), 307–313 (1992).
2. S. B. Kim and J.H. Park, "Optical see-through Maxwellian near-to-eye display with an enlarged eyebox," *Opt. Lett.* **43**(4), 767–770 (2018).
3. T. Zhan, J. Zou, J. Xiong, X. Liu, H. Chen, J. Yang, S. Liu, Y. Dong, and S.T. Wu, "Practical chromatic aberration correction in virtual reality displays enabled by cost-effective ultra-broadband liquid crystal polymer lenses," *Adv. Opt. Mater.* **8**(2), 1901360 (2020).
4. J. Xiong and S.T. Wu, "Planar liquid crystal polarization optics for augmented reality and virtual reality: from fundamentals to applications," *eLight* **1**(1), 3 (2021).
5. K. Gao, H.H. Cheng, A. Bhowmik, C. McGinty, and P. Bos, "Nonmechanical zoom lens based on the Pancharatnam phase effect," *Appl. Opt.* **55**(5), 1145–1150 (2016).
6. J. Kim, C. Oh, S. Serati, and M.J. Escuti, "Wide-angle, nonmechanical beam steering with high throughput utilizing polarization gratings," *Appl. Opt.* **50**(17), 2636–2639 (2011).
7. J. Xiong, G. Tan, T. Zhan, and S.T. Wu, "Breaking the field-of-view limit in augmented reality with a scanning waveguide display," *OSA Continuum* **3**(10), 2730–2740 (2020).

8. T. Zhan, J. Xiong, J. Zou, and S.T. Wu, "Multifocal displays: review and prospect," *Photonix* **1**(1), 10 (2020).
9. K. Yin, E.L. Hsiang, J. Zou, Y. Li, Z. Yang, Q. Yang, P.C. Lai, C.L. Lin, and S.T. Wu, "Advanced liquid crystal devices for augmented reality and virtual reality displays: principles and applications," *Light: Sci. Appl.* **11**(1), 161 (2022).
10. K. Yin, H.Y. Lin, and S.T. Wu, "Chirped polarization volume grating with ultra-wide angular bandwidth and high efficiency for see-through near-eye displays," *Opt. Express* **27**(24), 35895–35902 (2019).
11. W. Chen, Y. Yu, Q. Mu, C. Juan, Q. Wang, S. Li, S. Zhang, and L. Xuan, "Super-broadband geometric phase devices based on circular polarization converter with mirror symmetry," *Appl. Phys. Lett.* **119**(10), 101103 (2021).
12. C. Oh and M.J. Escuti, "Achromatic diffraction from polarization gratings with high efficiency," *Opt. Lett.* **33**(20), 2287–2289 (2008).
13. N.V. Tabiryani, S.V. Serak, S.R. Nersisyan, D.E. Roberts, B.Y. Zeldovich, D.M. Steeves, and B.R. Kimball, "Broadband waveplate lenses," *Opt. Express* **24**(7), 7091–7102 (2016).
14. J. Zou, T. Zhan, J. Xiong, and S.T. Wu, "Broadband wide-view Pancharatnam-Berry phase deflector," *Opt. Express* **28**(4), 4921–4927 (2020).
15. K. Yin, Z. He, K. Li, and S.T. Wu, "Doubling the FOV of AR display with a liquid crystal polarization-dependent combiner," *Opt. Express* **29**(8), 11512–11519 (2021).
16. Z. Zhuang, Y.J. Kim, and J.S. Patel, "Achromatic linear polarization rotator using twisted nematic liquid crystals," *Appl. Phys. Lett.* **76**(26), 3995–3997 (2000).
17. T.X. Wu, Y. Huang, and S.T. Wu, "Design optimization of broadband linear polarization converter using twisted nematic liquid crystal," *Jpn. J. Appl. Phys.* **42**(Part 2, No.1A/B), L39–L41 (2003).
18. Q.H. Wang, T.X. Wu, X. Zhu, and S.T. Wu, "Achromatic polarization switch using a film-compensated twisted nematic liquid crystal cell," *Liq. Cryst.* **31**(4), 535–539 (2004).
19. J. Xiong, Y. Li, K. Li, and S.T. Wu, "Aberration-free pupil steering Maxwellian display with wide-view broadband polarization converters," *J. Soc. Inf. Disp.* **29**(5), 298–304 (2021).
20. D.K. Yang and S.T. Wu, *Fundamentals of Liquid Crystal Devices*, (John Wiley & Sons, Ltd, 2015) pp. 102–110.
21. G.D. Love and R. Bhandari, "Optical properties of a QHQ ferroelectric liquid crystal phase modulator," *Opt. Commun.* **110**(5-6), 475–478 (1994).
22. Y. Ma, X. Liu, J. Sun, M.C. Tseng, and H.S. Kwok, "Ferroelectric liquid crystal devices on strengthened photoalignment films," *Liq. Cryst.* **47**(10), 1452–1457 (2020).